Journal of Nuclear Materials 390–391 (2009) 259–262

Contents lists available at ScienceDirect

Journal of Nuclear Materials

journal homepage: www.elsevier.com/locate/jnucmat

Impurity seeding and scaling of edge parameters in ITER

H.D. Pacher [a,*], A.S. Kukushkin [b], G.W. Pacher [c], V. Kotov [d], G. Janeschitz [e,1], D. Reiter [d], D.P. Coster [f]

[a] INRS-EMT, 1650 boul. Lionel Boulet, Varennes, QC, Canada J3X 1S2
[b] ITER Organization, Cadarache Centre, F-13108 St. Paul lez Durance, France
[c] Hydro_Québec, 1804, boul. Lionel Boulet, Varennes, QC J3X1S1, Canada
[d] IPP, Forschungszentrum Jülich, D-52425 Jülich, Germany
[e] Forschungszentrum Karlsruhe, P.O. Box 3640, D-76021 Karlsruhe, Germany
[f] Max-Planck-Institut für Plasmaphysik, Boltzmannstr. 2, D-85748 Garching bei München, Germany

ARTICLE INFO

PACS:
52.25.Ya
52.65.Kj
52.65.Pp
28.52.Av

ABSTRACT

ITER divertor and edge modelling with the ITER B2–EIRENE code including neutral–neutral and molecule–ion collisions has led to updated scaling of the helium density and flux and the DT flux with the pumping speed and the divertor neutral pressure. The replacement of carbon by the addition of seeded impurities (neon) strongly modifies the upstream DT density and DT neutral influx at constant detachment state, i.e. divertor neutral pressure and has a smaller influence on the peak divertor power load. The core plasma performance is modelled with the integrated core-pedestal–SOL (ICPS) model implemented in ASTRA; the operating window with seeded impurities is smaller than with DT injection alone.

1. Introduction

B2–EIRENE modelling has been applied extensively to model the ITER divertor with carbon divertor plates. We now use routinely the B2–EIRENE code package version solps4.2 [1–4], which relies on a nonlinear model of neutral particle transport, including neutral–neutral and molecule–ion collisions. The model assumptions are those of [1]. We fix the plasma power entering the scrape-off layer (SOL) at 100 MW, fix the D ion flow from the core across the core-edge interface (CEI) at 17 Pa m^3 s^{-1}, and vary the density with the flux injected by gas puffing. D_2 gas is puffed in, usually from the top, and pumped out via the duct in the private flux region at the bottom of the chamber. The plasma contains ions and atoms of D (representing both D and T), He, and C, as well as D_2 molecules. The present paper extends the previous simulations by (a) updating the scaling of the edge parameters (from that of [2]) for variations of DT flux and helium density and flux with pumping speed and neutral pressure, (b) removing carbon and introducing seed neon impurity to commence simulation of the later phase of ITER operation, and (c) determining the effect of the impurity seeding on the operating window of ITER following [5,6].

2. Scaling of edge parameters

In previous work ([2] and references therein) the key parameter for determining the edge plasma parameters was found to be,

$$\mu \equiv p_{\mathrm{DT\#}}\, P_{\#}^{-0.87}\, f_{\mathrm{f}}^{-0.8}\, f_{\mathrm{w}}^{-1}\, q_{95\#}^{-0.27}\, f_{\mathrm{nn}}^{-1}\, R_{\#}^{-1.21}. \quad (1)$$

This is proportional to $p_{\mathrm{DT\#}}$, the normalised average divertor neutral pressure at the entrance to the private flux region. Here $R_{\#}$ represents the normalised divertor radius, $P_{\#}$ the power entering the SOL normalised by $R_{\#}^3$, and $q_{95\#}$, the normalised safety factor. The normalisation factors are given in Table 1 of [2], as are the other factors depending on type of fuelling, wall, and neutral model, respectively f_{f}, f_{w} and f_{nn}. (Note that Table 1 of [2] contained an error: the normalisation factor of μ should be 1, and that of $p_{\mathrm{DT\#}}$ should be 8.5).

The edge-based density limit is taken to occur at detachment of the inner divertor ($\mu = 1$) because of increased neutral influx to the core beyond this point. As shown in [2] the DT separatrix density varies as $\mu^{0.43}$, i.e. the density analogue of μ is the ratio of the edge density to that at detachment, $f_{\mathrm{sat\_n}} = \mu^{0.43}$.

Initial results reported in [2] with the nonlinear neutral model indicated that the DT neutral flux was higher (factor 2) and the helium density and flux at the separatrix were lower (factor 0.33) than for the less complete linear neutral model but the scaling had then not yet been determined. We have now varied both pumping speed and throughput (i.e. $p_{\mathrm{DT\#}}$), with results in Fig. 1. Both the original dome F12 and a more recent smaller dome, F47 (see [4]) are shown, the latter with two different pumping speeds. The fit is performed taking into account all of the points in Fig. 1, and the fit values are then given for every one of these points.

The results can be well represented by:

$$\Gamma_{\mathrm{DT}} \equiv 36 f_{\mathrm{f}}^{-4.3}\, S_{\#}^{0.5} f_{\mathrm{w}}^{0.44}\, q_{95\#}^{-0.2} R_{\#}^{1.03}\, \mu^{0.7}\ [\mathrm{Pa\text{-}m^3\ s^{-1}}], \quad (2)$$

* Corresponding author.
E-mail address: pacher@emt.inrs.ca (H.D. Pacher).
[1] Present address: ITER Organization, Cadarache Centre, F-13108 St. Paul lez Durance, France.

0022-3115/$ - see front matter Crown Copyright © 2009 Published by Elsevier B.V. All rights reserved.
doi:10.1016/j.jnucmat.2009.01.089

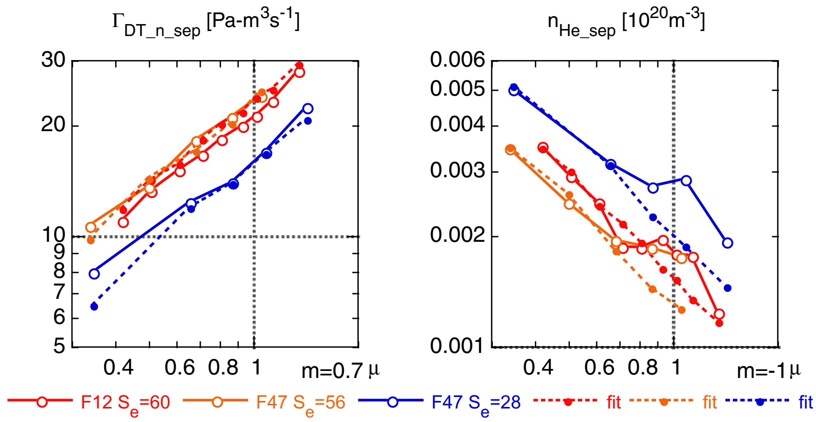

Fig. 1. DT neutral flux (a, left) and helium density (b, right) at the separatrix versus μ (Eq. (1) and text), proportional to DT neutral pressure in the divertor, for two different dome configurations (F12 and F47, see text) and engineering pumping speed S_e in $m^3 s^{-1}$: 60 (F12), 56 (F47) and 28 (F47). 'Fit' are the values from Eqs. (2) and (3) at low-μ.

$$
\begin{aligned}
&n_{He\_sep} = k_{n\_He}\mu^{-1} && \text{for } \mu < 0.65,\\
&k_{n\_He}\mu^{-1}t < n_{He\_sep} < k_{n_{He}}(0.65)^{-1} && \text{for } 0.65 < \mu < 1,
\end{aligned}
\tag{3}
$$

where $k_{n\_He} = 0.001 f_{He} f_f^{-4} S_\#^{-0.7} \xi_{ei}^{-0.1} q_{95\#}^{-0.85} P_\#^{0.79} R_\#^{0.15}$ $[10^{20}\ m^{-3}]$.

$$
\begin{aligned}
&\Gamma_{He\_n\_sep} = k_{\Gamma\_He}\mu^{-0.86} && \text{for } \mu < 0.65,\\
&k_{\Gamma\_He}\mu^{-0.86} < \Gamma_{He\_n\_sep} < k_{\Gamma\_He}(0.65)^{-0.86} && \text{for } 0.65 < \mu < 1,
\end{aligned}
\tag{4}
$$

where $k_{\Gamma\_He} \equiv 0.08 f_{He} f_f^{-2} S_\#^{-0.7} P_\#^{0.22} R_\#^{-1.46}$ $[Pa\ m^3\ s^{-1}]$.

Here $S_\#$ is the engineering pumping speed for D2 molecules at the duct entrance, normalised to $114\ m^3\ s^{-1}$ (see discussion in [3], Section 2).

These low-μ fits extrapolated to $\mu = 1$ for dome F12 are close to the preliminary factors of [2] relative to the less complete linear neutral model, i.e. 2.44, 0.37, and 0.3 for DT flux, helium density, and helium flux, respectively. The variation with pumping speed and with μ is stronger for the DT flux and weaker for the helium quantities than for the linear model, and, importantly the helium quantities increase much less rapidly toward lower DT pressure than the previous scaling based on the linear model (exponents 1 and 0.86 rather than 2 and 2). As seen in Fig. 1, the smaller dome F47 results in slightly lower helium levels. For the more complete nonlinear model, the helium quantities depart from the low-μ fits above $\mu > 0.65$, are up to 50% higher at $\mu = 1$, and then decrease again.

3. Effect of neon impurity seeding on the edge and divertor plasma

Impurity seeding is useful to reduce the peak power load on a future carbon-free divertor. We have varied the neon concentrations at the separatrix in the range $0.001 < c_{Ne} < 0.03$. In order not to vary too many parameters simultaneously, for this study we have used the same particle and energy reflection coefficients at the wall as for carbon, but with zero carbon erosion. Further studies with the parameters appropriate for tungsten will follow. (A variant, several runs with neon, full beryllium walls and self-consistent beryllium sputtering, yielded low Be concentration $c_{Be} \sim 0.005$ and low Be radiated power 2–4 MW, with other values similar to the carbon-free cases with neon so that this will not be discussed further.)

The resulting radiated power for dome F12 (Fig. 2(a)) varies little with c_{Ne} for $c_{Ne} > 0.01$, and is slightly below the radiation in the carbon case. However (Fig. 2(b)) the radiation in the inner divertor volume for the Ne cases is 2/3 the value for the C case at $\mu = 1$, down to 1/3 at lower pressures (for the outer divertor volume, the corresponding values are 100% and 80%). This is attributed to the energy-independent chemical erosion for the C case and the low radiation of neon below 10 eV. The plasma at the inner divertor target remains somewhat hotter (Fig. 3(a)) and the power to that target is higher than with C for $\mu < 1$. Detachment is described by the same μ for C and Ne, i.e. no additional factor is required. Whereas for C and for neon at low c_{Ne} the power maximum is on the outer divertor plate, it is on the inner divertor plate for $c_{Ne} > 0.01$ and $\mu < 1$. For the inner target with neon, the scaling is similar to that for the outer target with carbon, but the numerical value is 30% lower and independent of c_{Ne} in this range. (Since the maximum does not occur on the same divertor plate as for C, differences in flux expansion, divertor plate angle, and divertor length also play a role). Therefore, to a good approximation,

$$q_{pk}|^{Ne} = 0.7 q_{pk}|^{C}. \tag{5}$$

With the nonlinear neutral model, $q_{pk}|^{C}$ is given by the scaling of [2] for dome F47, and 1.2 times this scaling for the older dome F12.

The DT density varies strongly with c_{Ne} at given throughput (i.e. the same μ), Fig. 4(a). As c_{Ne} increases for $c_{Ne} \geqslant 0.01$, the power available for DT dissociation, ionisation, and excitation decreases and n_{DT} decreases. To a very good approximation (Fig. 4(b)),

$$n_{DT\_sep}|^{Ne} + 40 n_{Ne\_sep}|^{Ne} = 1.45 n_{DT\_sep}|^{C} \mu^{-0.34} \quad \text{for } c_{Ne} \leqslant 0.01, \tag{6}$$

$n_{DT\_sep}|^{C}$ is given by the scaling of [2] for dome F47, $\sim\mu^{0.43}$, and 0.8 times this scaling for the older dome F12.

Neon is ionised to 8.8 at the separatrix, and the total ionisation energy required to attain this state is about 100 times that of DT per atom. Given the profiles of Z, different residence times and different ratios of excitation to ionisation of Ne and DT, the factor 40 in Eq. (6) is broadly consistent with this ratio. The decrease in n_{DT} engenders a strong decrease in n_e, albeit somewhat smaller (80% over the range shown) than that of n_{DT}, and this in turn is responsible for the fact that the radiated power is almost invariant with c_{Ne} for $0.01 < c_{Ne} < 0.03$.

As the neon concentration increases, the helium density and neutral flux at the separatrix progressively decrease by factors of 2.2 and 7.5, respectively, below Eqs. (3) and (4). This is tentatively attributed to lower DT and electron densities in the divertor plasma, leading to lower opacity of this plasma to neutrals and more efficient pumping (the reduction of helium is stronger in the inner divertor), but the details remain to be worked out.

4. Operating diagram

The scaling relations of [2] and the present updated values, including those for neon seeding, from Eqs. (1)–(5), are input